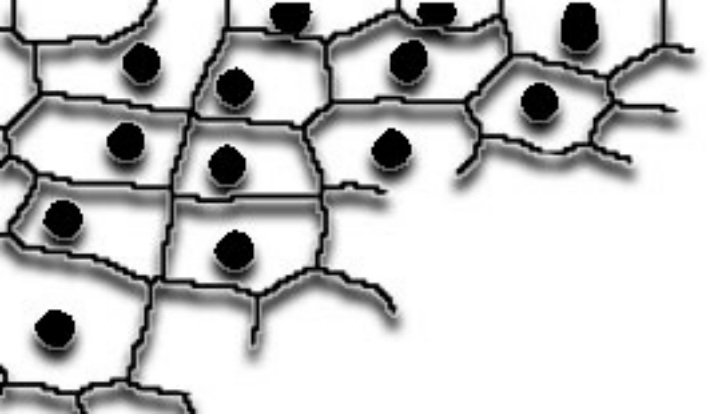

4

Noonan Syndrome Gain-of-Function Mutations in NRAS cause Zebrafish Gastrulation Defects

Vincent Runtuwene*, Mark van Eekelen*, John Overvoorde, Holger Rehmann, Helger G. Yntema, Willy M. Nillesen, Arie van Haeringen, Ineke van der Burgt, Boudewijn Burgering and Jeroen den Hertog

Dis Model Mech. 2011 May; 4(3): 393–399.

*=equal contribution

Abstract

Noonan syndrome is a relatively common developmental disorder that is characterized by reduced growth, wide-set eyes and congenital heart defects. Noonan syndrome is associated with dysregulation of the Ras–mitogen-activated-protein-kinase (MAPK) signaling pathway. Recently, two mutations in *NRAS* were reported to be associated with Noonan syndrome, T50I and G60E. Here, we report a mutation in *NRAS*, resulting in an I24N amino acid substitution, that we identified in an individual bearing typical Noonan syndrome features. The I24N mutation activates N-Ras, resulting in enhanced downstream signaling. Expression of N-Ras-I24N, N-Ras-G60E or the strongly activating mutant N-Ras-G12V, which we included as a positive control, results in developmental defects in zebrafish embryos, demonstrating that these activating N-Ras mutants are sufficient to induce developmental disorders. The defects in zebrafish embryos are reminiscent of symptoms in individuals with Noonan syndrome and phenocopy the defects that other Noonan-syndrome-associated genes induce in zebrafish embryos. MEK inhibition completely rescued the activated N-Ras-induced phenotypes, demonstrating that these defects are mediated exclusively by Ras-MAPK signaling. In conclusion, mutations in *NRAS* from individuals with Noonan syndrome activated N-Ras signaling and induced developmental defects in zebrafish embryos, indicating that activating mutations in *NRAS* cause Noonan syndrome.

Introduction

Activating mutations in genes encoding components of the Ras-MAPK pathway have not only been identified in various tumor types, but also in developmental disorders (Aoki et al., 2008; Karnoub and Weinberg, 2008; Schubbert et al., 2007). Germline mutations in genes of the Ras-MAPK pathway have been found in a group of genetic syndromes that are collectively called RASopathies, including Noonan syndrome (OMIM 163950), LEOPARD syndrome (OMIM 151100), Costello syndrome (OMIM 218040) and cardio-facio-cutaneous (CFC) syndrome (OMIM 115150) (Denayer et al., 2008; Tidyman and Rauen, 2009). These syndromes are characterized by partially overlapping symptoms, including distinctive craniofacial features and cardiovascular anomalies, and they are genetically heterogeneous, with mutations in known disease genes accounting for 70–80% of the cases.

Noonan syndrome is a relatively common dominantly inherited genetic disorder characterized by congenital heart defects, reduced growth, facial dysmorphism and variable congenital defects (Gelb and Tartaglia, 2006). The syndrome is caused by activating mutations in genes encoding upstream factors of the Ras-MAPK pathway, including *PTPN11* (*Shp2*) (Tartaglia et al., 2001) and *SOS1* (Roberts et al., 2007; Tartaglia et al., 2007), as well as *KRAS* (Pandit et al.,

2007; Schubbert et al., 2006), *SHOC2* (Cordeddu et al., 2009) and the more downstream signal transducers *RAF1* and *BRAF* (Pandit et al., 2007; Razzaque et al., 2007; Tartaglia et al., 2007). The most recent addition to the group of genes that are associated with Noonan syndrome is *NRAS*. In a cohort of 917 individuals with typical features of Noonan syndrome, who were negative for mutations in previously known Noonan-syndrome-associated genes, two distinct mutations, T50I and G60E, were identified in *NRAS* in four individuals. Mutant N-Ras-G60E and, to a lesser extent, N-Ras-T50I activated MAPK signaling in cells (Cirstea et al., 2010). Activation of N-Ras was previously found to be associated with acute myeloid leukemia (AML) (Bos et al., 1985; Bos et al., 1987) and melanoma (van 't Veer et al., 1989), and a germline activating mutation in *NRAS* causes autoimmune lymphoproliferative syndrome (Oliveira et al., 2007).

Here, we report the identification of a new mutation in N-Ras in an individual with Noonan syndrome that results in an amino acid substitution, I24N. Mutant N-Ras-I24N activates downstream MAPK signaling. We used zebrafish embryos to assess the *in vivo* effects of dominant mutations in genes that are associated with Noonan syndrome, as we and others have done previously (Anastasaki et al., 2009; Jopling et al., 2007; Razzaque et al., 2007; Stewart et al., 2010). Expression of N-Ras-I24N or two other Noonan-syndrome-associated N-Ras mutants, T50I or G60E, in zebrafish embryos resulted in severe developmental defects during epiboly and gastrulation that resemble the defects observed in response to a known Noonan-associated gene. Interestingly, pharmacological inhibition of MEK rescued these activated N-Ras-induced developmental defects, demonstrating that the activated N-Ras-induced defects are caused by activation of MAPK signaling.

Results and Discussion

In search of the genetic cause of Noonan syndrome, we resequenced all exons of *NRAS* in a Dutch cohort of 56 Noonan syndrome patients lacking mutations in known Noonan-syndrome-associated genes. We found a single individual heterozygous for a nucleotide mutation in exon 2, c.71T>A, resulting in the amino acid substitution p.I24N (Fig. 1A). The 30-year-old patient had been diagnosed with Noonan syndrome and demonstrated the facial features, low posterior hairline, webbing of the neck, pectus excavatum, cryptorchism, mild learning difficulties and mild short stature characteristic of the syndrome. Assessment at birth and at age 15 revealed no heart abnormalities. His parents did not exhibit classical Noonan features and did not harbor the mutation in *NRAS* (Fig. 1Ab,c), demonstrating the *de novo* origin of the mutation. To exclude the possibility of somatic mosaicism, *NRAS* was resequenced in skin fibroblasts and buccal epithelial

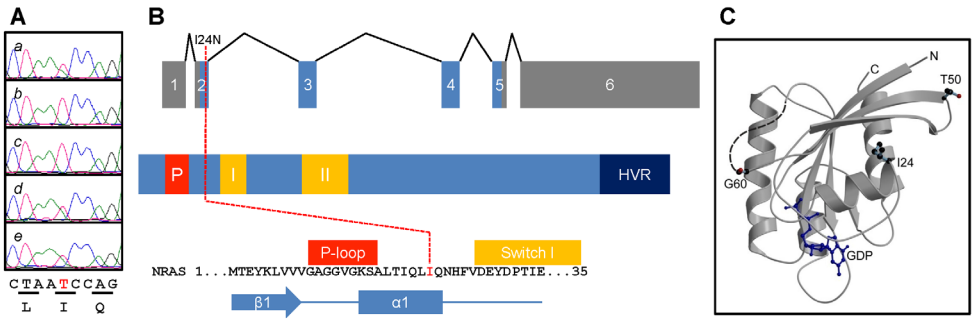

Figure 1. Identification and localization of an I24N amino acid substitution in N-Ras in an individual with typical features of Noonan syndrome.
(A) The heterozygous c.71T>A nucleotide substitution in exon 2 that was first identified in the patient (a) was not detected in the father (b) or the mother (c) and was detected in DNA isolated from fibroblasts (d) and sputum (e) of the patient. (B) Genomic organization (top), protein structure (middle) and sequence of N-Ras around Ile24 (bottom), which is encoded by exon 2, which is located on helix α1, between the P-loop (P) and switch I (I). Switch II (II) and the hypervariable region (HVR) are also indicated in the protein structure. (C) Ribbon representation of N-Ras•GDP (Protein Data Bank code: 3con), with GDP (blue) and residues Ile24, Thr50 and Gly60 highlighted as ball and stick representation. Missing connectivity for residues 61 to 71 is indicated by a dotted line.

cells from sputum from the patient, both of which showed the c.71T>A mutation heterozygously (Fig. 1Ad,e), which supports the conclusion that the patient has a germline *NRAS* mutation. The c.71T>A mutation was not found in 100 controls without Noonan syndrome.

The surrounding sequence of I24 is identical in N-Ras, K-Ras and H-Ras, and is localized between the P-loop, involved in nucleotide binding, and Switch I, involved in effector binding (Fig. 1B). Mutations in I24 have not previously been identified in any Ras isoform. Whereas efficient GTP hydrolysis is blocked in oncogenic Ras with G12V or Q61K mutations, resulting in activated Ras, such an effect of I24N is unlikely, given the location of I24 in N-Ras (Fig. 1B,C). Recently, H-Ras mutations in Gln22 (Q22) were described in three patients diagnosed with RASopathies, specifically Noonan syndrome (Q22R), CFC syndrome (Q22E) and Costello syndrome (Q22K) (van der Burgt et al., 2007; Zenker et al., 2007). Although biochemical data that the Q22 mutations activate H-Ras was not provided, other patients with similar symptoms contained well-known activating mutations in H-Ras, including G12V, G12S, G60R or E63K. Hence, it is likely that the Q22 mutations activate H-Ras, suggesting an important regulatory role for the region between the P-loop and Switch I, which includes N-Ras I24 (Fig. 1B).

Two mutations in *NRAS* were previously identified in Noonan syndrome patients, one of which (G60E) is characterized as highly GTP bound, whereas the other (T50I) showed normal GTP loading (Cirstea et al., 2010). To assess the activation state of N-Ras-I24N, GTP-bound Ras was selectively precipitated from cells stimulated with serum. We found that a higher proportion of N-Ras-I24N was precipitated relative to wild-type N-Ras (Fig. 2A). A similar effect was observed for N-Ras-G12V and N-Ras-G60E, but not for N-Ras-T50I. In the absence of serum, out of these mutants only oncogenic N-Ras-G12V was highly GTP bound. These results group N-Ras-I24N in the class of 'mild activating' mutations, the activation of which is dependent on upstream signaling. Mild activating mutations are commonly associated with Noonan and Noonan-related syndromes (Tidyman and Rauen, 2009). The side chain of Ile24 (I24) in the α1-helix points towards the β2-strand (Fig. 1C) and mutation to Asn (N) would probably result in repulsing forces between the α1-helix and the β2-strand, thereby destabilizing the fold of the G protein. Hence, the nucleotide affinity might be weakened, resulting in an increased exchange rate and therefore higher GTP loading under physiological conditions, because the GTP:GDP ratio is ~9:1 in cells. This would be in agreement with the 'mild activation' character of the I24N mutant.

We next investigated MAPK activation, a downstream consequence of N-Ras activation, in 293T cells expressing N-Ras-I24N and found robust MAPK

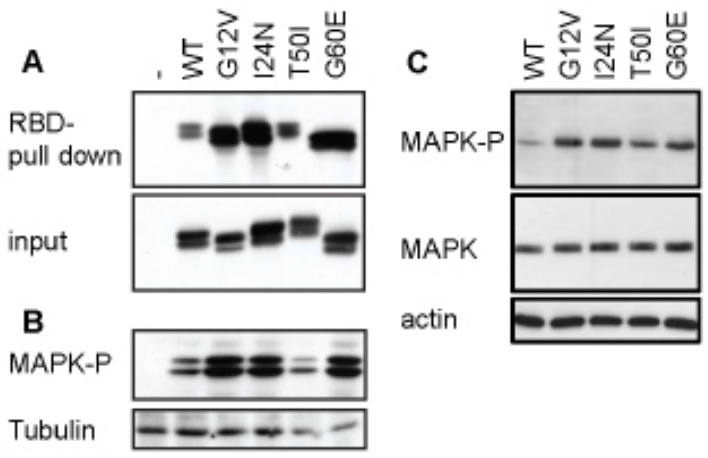

Figure 2. I24N mutation activates N-Ras and downstream signaling. (A) Active, GTP-bound Ras was selectively precipitated from lysates of growing 293T cells transfected with RNA encoding N-Ras (wild type or mutants) with the Ras-binding domain (RBD) of Raf-1. Precipitated Ras was detected by immunoblotting using a Ras-specific antibody. The amount of Ras in the lysates was monitored by immunoblotting. (B) Transfected, growing 293T cells expressing N-Ras (mutants) were lysed and equal amounts of these lysates were loaded onto SDS-PAGE gels, blotted and probed with antibody against phospho-MAPK, or against Tubulin as a loading control. (C) Synthetic RNA (5 pg) encoding wild-type or mutant N-Ras was injected into zebrafish embryos at the one-cell stage. Embryos were lysed at 24 hpf and loaded onto SDS-PAGE gels, blotted and probed with antibodies against phospho-MAPK, MAPK and, as a loading control, against actin.

phosphorylation in the presence of serum in comparison with wild-type N-Ras (Fig. 2B). N-Ras-G60E and the positive control, N-Ras-G12V, also enhanced MAPK activation, but N-Ras-T50I did not, which is in agreement with a weak or no increase in Ras-binding domain (RBD) binding (Fig. 2A). Together, these results demonstrate that the I24N amino acid substitution increases the fraction of active N-Ras and enhances MAPK activation, which might be due to enhanced GTP loading from subtle changes in the conformation of the GTP-binding pocket.

To evaluate the functional consequences of activating mutations in Noonan-syndrome-associated genes at the organismal level, we and others have used zebrafish as a model system (Anastasaki et al., 2009; Jopling et al., 2007; Razzaque et al., 2007; Stewart et al., 2010). Mutant N-Ras was expressed in zebrafish embryos at the one-cell stage by injection of synthetic RNA encoding wild-type or mutant N-Ras. We first established that MAPK phosphorylation is enhanced in response to N-Ras-I24N, N-Ras-G60E and N-Ras-G12V, relative to wild-type N-Ras in zebrafish embryos (Fig. 2C), which is consistent with our results in 293T cells (Fig. 2B). N-Ras-T50I only weakly activated MAPK phosphorylation in zebrafish embryos.

Morphological defects in embryos expressing mutant forms of N-Ras were apparent at 11 hours post-fertilization (hpf). The morphology of the *nras*-injected embryos was monitored by time-lapse imaging. Notably, N-Ras-I24N seemed to induce epiboly and gastrulation defects, as reflected in the reduced body axis extension at 14 hpf (supplementary material Fig. S1) and the oval shape of the embryos at epiboly (Fig. 3A). Severe morphological defects were not observed at 11 hpf or 24 hpf in embryos injected with RNA encoding wild-type N-Ras. The morphological phenotypes induced by N-Ras-I24N at 24 hpf ranged in severity from completely disorganized embryos to mildly affected shorter embryos (Fig. 3A).

The epiboly defects were quantified by analysis of the ratio of the major and minor embryonic axes (Fig. 3B). Non-injected control embryos were almost perfect spheres and the ratio of the major and minor embryonic axes was approximately 1. Injection of RNA encoding N-Ras-I24N resulted in a significant increase in the major:minor axis ratio, whereas the ratio with wild-type N-Ras was similar to non-injected controls. N-Ras-G12V from tumors and N-Ras-G60E from Noonan patients both strongly affected the major:minor axis ratio, whereas N-Ras-T50I only had mild effects (Fig. 3C). Activating mutants in B-Raf were recently reported to induce defects in epiboly (Anastasaki et al., 2009); thus, we included the robustly active B-Raf-V600E mutant as a positive control in our assay. As expected, this mutant exerted a strong effect on the major:minor axis ratio, whereas wild-type B-Raf had no effect (Fig. 3C).

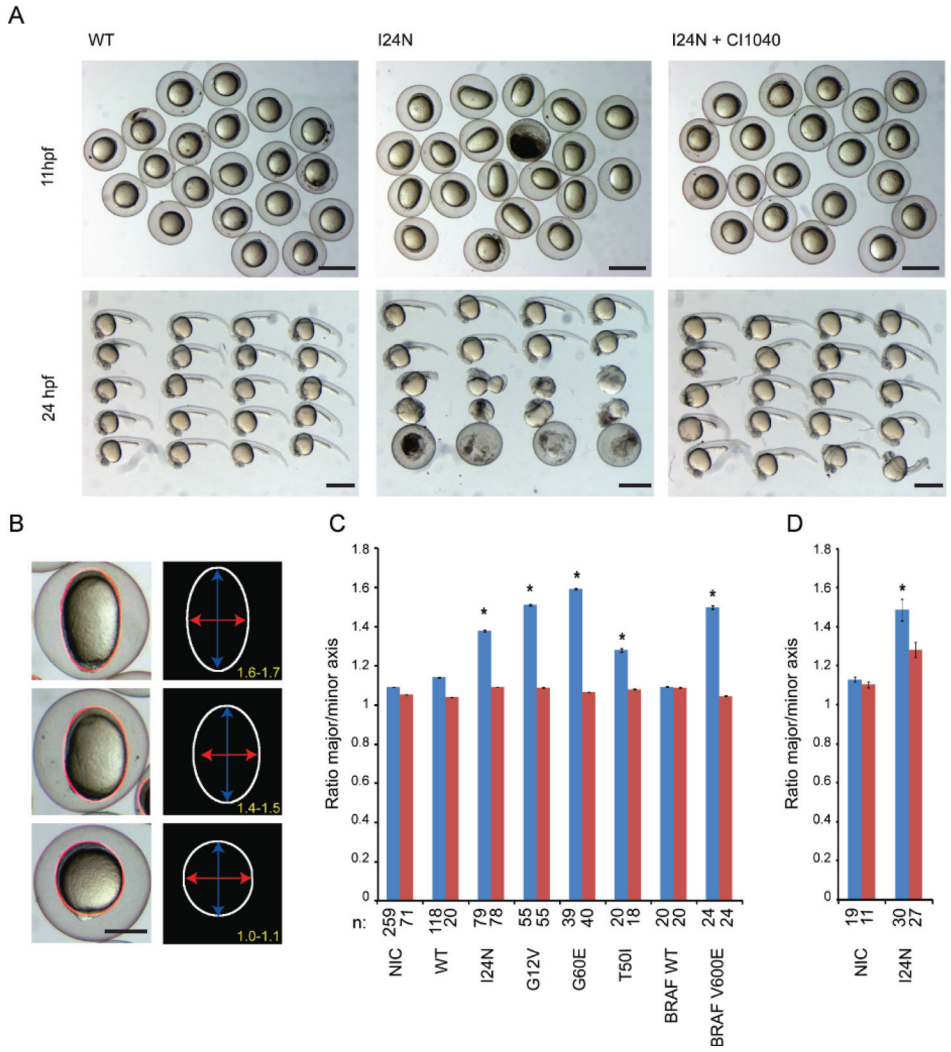

Figure 3. Active N-Ras-induced early developmental defects in zebrafish embryos.
(A) Embryos were injected at the one-cell stage with synthetic RNA (5 pg) encoding N-Ras (wild type or mutant), and morphology was assessed at 11 hpf and 24 hpf. Injected embryos were incubated with MEK inhibitor CI-1040 (1 μM) from 4.5 hpf until 5.5 hpf. Representative batches of embryos are depicted here. Scale bars: 1 mm. (B) The severity of the phenotype was determined by assessment of the shape of the embryos at 11 hpf. The ratio of the length of the major and minor axes was determined, as indicated in examples of severely affected (top), mildly affected (middle) and a control (bottom) embryos. Scale bar: 500 μm. (C) Quantification of the ratio of the major and minor axes upon injection of synthetic RNAs encoding wild-type (WT) or mutant N-Ras as indicated. As a negative control, the major:minor axis ratio was determined in non-injected control embryos (NIC). In addition, RNA encoding wild-type B-Raf or activated mutant B-Raf-V600E was injected. Blue bars: embryos were mock treated (0.1% DMSO); red bars: embryos were treated with MEK inhibitor CI-1040 (1 μM). (D) Embryos were treated with the FGFR inhibitor SU5402 (5 μM) from 4.5 hpf onwards and the phenotype was quantified as in C. Blue bars: mock-treated

(0.1% DMSO); red bars: FGFR-inhibitor-treated. Averages of the major:minor axis ratio are depicted in panels C and D and the s.e.m. is indicated; Student's t-tests (two-tailed, assuming unequal variance) were performed between mutant and wild-type N-Ras-injected groups; *P<0.001. The total number of embryos from two to six independent experiments that were used per condition are indicated (n).

The effects of the N-Ras mutants on early zebrafish development were probably due to activation of the MAPK pathway. Using the MEK inhibitor CI-1040 to suppress downstream MAPK activation, we found that the deleterious effects of N-Ras-I24N on epiboly and later development were completely rescued by inhibition of MEK (Fig. 3A). Quantification of the epiboly defects confirmed the complete rescue of the N-Ras-I24N, N-Ras-G12V, N-Ras-G60E and N-Ras-T50I mutants, as well as B-Raf-V600E (Fig. 3C). Taken together, our data demonstrate that N-Ras-I24N is a functionally activated mutant of N-Ras that induces developmental defects, similar to those induced by N-Ras-G12V and N-Ras-G60E in a pathway requiring N-Ras-mediated activation of MAPK. It should be noted that the rescues were mediated by a pulse of MEK inhibitor between 4.5 and 5.5 hpf, whereas a more prolonged exposure to the inhibitor induced developmental defects on its own, consistent with a previous report (Anastasaki et al., 2009).

N-Ras-I24N is a mildly activating mutant of N-Ras, which requires serum to be present for activation of the Ras-MAPK pathway in 293T cells (Fig. 2B). Fibroblast growth factor receptor (FGFR) signaling is an upstream factor in convergence and extension cell movements during gastrulation. We assessed the effect of the FGFR inhibitor SU5402 on N-Ras-I24N-induced developmental defects. Interestingly, we observed that SU5402 partially rescued the gastrulation defects that were induced by N-Ras-I24N, whereas SU5402 at these concentrations had no effect on non-injected control embryos (Fig. 3D). We conclude that upstream FGFR signaling is required for the developmental defects that are induced by N-Ras-I24N.

To further characterize the activated N-Ras-induced epiboly and gastrulation cell-movement defects, we used classical molecular markers for *in situ* hybridization. Convergence and extension cell movements during gastrulation shape the embryos, making the embryo narrower (convergence) and longer (extension) (Solnica-Krezel, 2006). A well-known marker for convergence and extension cell movements during gastrulation is the ratio between the width of the *krox20*-positive rhombomeres 3 and 5 and the distance between somites 1 and 8, visualized by *myoD* staining at the eight-somite stage (12 hpf) (Li et al., 2008). Injection of N-Ras-I24N led to widening of the embryos at 12 hpf (Fig. 4A). N-Ras-G12V and N-Ras-G60E had extreme effects, whereas N-Ras-T50I resembled wild-type N-Ras (Fig. 4A). Quantification of the ratio of the width to the length

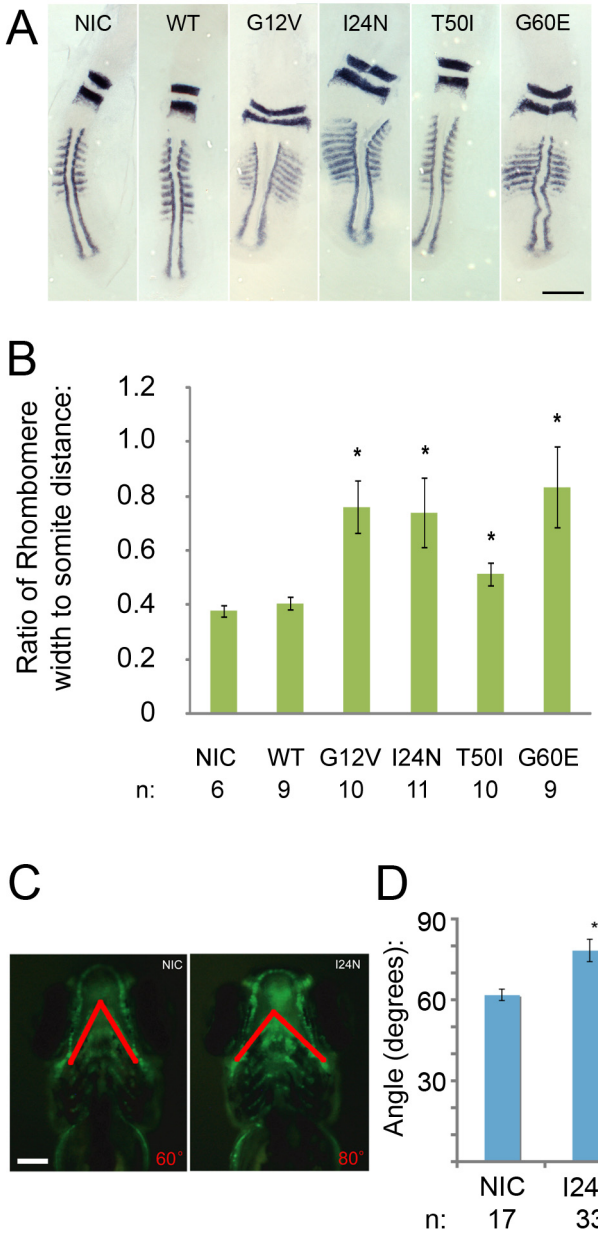

Figure 4. Active N-Ras induced convergence and extension cell-movement defects and craniofacial defects.
(A) In situ hybridization was performed using embryos at the eight-somite stage (~12 hpf) using *krox20* and *myod*-specific probes: non-injected control (NIC) embryos or embryos injected with synthetic RNA encoding wild-type (WT) N-Ras or mutants, as indicated, were used. Dorsal views of flat-mounted embryos are depicted, anterior to the top. Scale bar: 250 µm. (B) The ratio of the width of the krox20 staining and the length from the first to the eighth somite was determined using ImageJ software and is depicted here. Error bars indicate s.e.m.; Student's t-tests (two-tailed, assuming unequal variance) were performed between mutant and wild-type N-Ras-injected groups; *P<0.005. Total numbers of embryos that were used for the analyses are indicated (n). (C) Embryos from the transgenic *Tg(–4.9sox10:EGFP)*^{ba} line, in which neural crest cells are marked, were injected at the one-cell stage with RNA encoding N-RAS-I24N. The ceratohyal is marked by GFP in the transgenic embryos at 4 dpf and lines (red) were drawn demarcating the ceratohyal, facilitating analysis of the angle in the ceratohyal, which is a direct marker for the width and bluntness of the heads of these embryos. Representative images of a non-injected control (NIC) and a N-RAS-I24N-injected embryo are depicted. Scale bar: 100 µm. (D) Quantification of the angle of the ceratohyal. The number of individuals used (n) is indicated. A Student's t-test was performed; asterisk indicates significant difference, P<0.005.

revealed significant increases in this ratio in embryos injected with RNA encoding mutant N-Ras-G12V, N-Ras-I24N and N-Ras-G60E, compared with wild-type *nras*-injected and non-injected controls (Fig. 4B). N-Ras-T50I also induced a significant albeit small increase in the ratio, relative to wild-type N-Ras. Another marker for convergence and extension cell movements is *dlx3* and *hgg1* staining

at the one-somite stage (10 hpf) (Jopling and den Hertog, 2005; van Eekelen et al., 2010). These markers indicate that N-Ras-G12V, N-Ras-I24N and N-Ras-G60E induced significant defects in convergence and extension cell movements as well (supplementary material Fig. S2). Taken together, these results demonstrate that activating N-Ras mutants induce gastrulation cell-movement defects at severities that parallel the capacity to activate MAPK.

To monitor gastrulation cell movements directly, we have developed time-lapse fluorescent microscopy of zebrafish embryos injected with fluorescent Histone H1 protein, which labels all nuclei (van Eekelen et al., 2010). Using this cell tracking technology, we found that expression of N-Ras-I24N resulted in a 10% reduction in convergence and 6% reduction in extension of paraxial mesendodermal cells, compared with embryos injected with RNA encoding wild-type N-Ras. These results are statistically significant ($P << 0.001$) because they are based on more than 1000 cell tracks each. One of the underlying mechanisms of convergence and extension is cell intercalation and mediolateral elongation (Concha and Adams, 1998; Myers et al., 2002). By cell membrane labeling and ratiometric analysis of cell shape and orientation, we found that cell polarization is reduced upon N-Ras-I24N expression (supplementary material Fig. S3), which is consistent with the observed convergence and extension cell-movement defects.

One of the hallmarks of Noonan syndrome is hypertelorism and we have demonstrated before that expression of mutant Shp2 leads to craniofacial defects, including wide-set eyes, in zebrafish embryos (Jopling et al., 2007). We assessed defects in craniofacial cartilage structures using the transgenic *Tg(−4.9sox10:EGFP)*^{ba2} zebrafish line, which expresses GFP in all neural crest cells (Carney et al., 2006). The angle of the ceratohyal is a direct measure for the width and the bluntness of the head (Fig. 4C), and is an excellent marker for hypertelorism. Expression of N-Ras-I24N led to a significant increase in the angle of the ceratohyal ($P<0.05$; Student's *t*-test) (Fig. 4C,D) and hence we conclude that N-Ras-I24N expression induced craniofacial defects in zebrafish embryos that are reminiscent of the symptoms in individuals with Noonan syndrome.

In conclusion, we report an activating mutation in N-Ras, I24N, that is associated with Noonan syndrome. Interestingly, our *in vivo* data in zebrafish embryos (Figs 3, ,4) demonstrate for the first time that the activating N-Ras mutants, I24N and G60E, are sufficient for inducing developmental defects that resemble the defects induced by active mutants of downstream factors, B-Raf, Raf-1 and MEK, from Noonan and related syndromes (Anastasaki et al., 2009), and hence firmly establish *NRAS* as a gene that causes Noonan syndrome upon activation. The observed craniofacial defects in zebrafish embryos (Fig. 4C,D) actually resemble symptoms in individuals with Noonan syndrome. Taken together, our *in*

vivo data demonstrate that *NRAS* is a bona fide Noonan-associated gene that has a causal role in the syndrome.

Ras mutations found in human cancer are thought to contribute to disease by activating at least three major downstream signaling pathways, i.e. the Raf-MAPK pathway, the PI3K-PKB/AKT pathway and the RalGDS-Ral pathway. In the case of Noonan N-Ras mutants, it becomes apparent that Raf-MAPK activation is sufficient. Mutational activation of B-Raf causes developmental defects in zebrafish that are identical to those in the activating N-Ras mutants, and pharmacological inhibition of MEK using CI-1040 completely rescues these developmental defects. MEK and/or MAPK inhibitors are currently in clinical trials for the treatment of cancers harboring active *RAS* mutations. This raises the interesting possibility that these inhibitors might also be appropriate for the treatment of developmental disorders that are caused by *RAS* mutations that depend exclusively on Raf-MAPK activation to convey their pathology.

Translational impact

Clinical issue

Noonan syndrome is a relatively common, dominantly inherited genetic disorder characterized by congenital heart defects, reduced growth, facial dysmorphism and other variable congenital defects. The syndrome is caused by activating mutations in genes encoding factors of the RAS-MAPK signaling pathway and hence belongs to a group of genetic syndromes that are collectively called RASopathies. Mutations in known disease-associated genes are found in 70–80% of patients with Noonan syndrome, and ~50% of patients have activating mutations in a gene encoding an upstream factor in the RAS-MAPK pathway [protein-tyrosine phosphatase, non-receptor type 11 (SHP2), encoded by *PTPN11*]. The most recent addition to the group of genes that are associated with Noonan syndrome is *NRAS*, which encodes a member of the Ras protein family.

Results

In this study, the authors report on a mutation in *NRAS* resulting in an I24N amino acid substitution that they identified in an individual bearing typical Noonan syndrome features. The I24N mutation mildly activates N-Ras, resulting in enhanced downstream signaling, similar to other activating N-Ras mutations that are associated with Noonan syndrome. By using zebrafish embryos as a model, they go on to show that expression of I24N or other disease-associated activat-

ing N-Ras mutants causes developmental defects, including cell migration defects during gastrulation. The craniofacial defects observed in the zebrafish embryos carrying disease-associated mutations in N-Ras resemble the defects observed in individuals with Noonan syndrome. Furthermore, developmental defects induced by activated N-Ras phenocopy the developmental defects that are induced by the expression of other genes known to be associated with Noonan syndrome, including *PTPN11*, in zebrafish embryos. Finally, they show that pharmacological inhibition of MEK, a downstream factor in the RAS-MAPK pathway, rescues the phenotype induced by activating N-Ras mutations, demonstrating that the observed defects are mediated exclusively by enhanced activation of the RAS-MAPK signaling pathway.

Implications and future directions

This study provides new evidence that *NRAS* is a bona fide Noonan-syndrome-associated gene and, moreover, that activation of N-Ras can cause the clinical phenotype. Hence, *NRAS* should be included in diagnostic screening for mutations in individuals with symptoms of Noonan syndrome. Notably, pharmacological inhibition of MEK rescues the developmental defects that are induced by activated N-Ras. Given that the RAS-MAPK pathway is also implicated in cancer, developing inhibitors of this pathway has been a major focus of many pharmaceutical companies, and clinical trials to test them in a subset of cancer patients are currently underway. Such inhibitors might also be effective for treating some RASopathies, including Noonan syndrome, that are caused by hyperactivation of the RAS-MAPK pathway.

Methods

Experimental subjects

Written informed consent was obtained from all subjects and/or their legal representatives, and the work was done according to the guidelines of the medical ethical committee of Radboud University, Nijmegen, The Netherlands.

All procedures involving experimental animals were performed in compliance with local animal welfare laws, guidelines and policies.

DNA isolation and sequencing

DNA was isolated from blood, fibroblasts or sputum. Mutational screening of *NRAS* (ENSG00000213281) was performed by PCR of all four exons, using the following primers: NRAS-1-F 5′-CGCCAATTAACCCTGATTAC-3′; NRAS-1-R 5′-AGAGAC-AGGATCAGGTCAGC-3′; NRAS-2-F 5′-ATAGCATTGCA-TTCCCTGTG-3′; NRAS-2-R 5′-CACAAAGATCATCCTT-TCAGAG-3′; NRAS-3-F 5′-CCACTGTACCCAGCCTAATC-3′;NRAS-3-R5′-AAACTCTTGCACAAATGCTG-3′;NRAS-4-R 5′-CCTCCAAATTGCCCAATAC-3′; NRAS-4-F 5′-ATTTG-GATTGTGTCCGTTG-3′.

Bidirectional resequencing was performed using a commercial sequencing kit (ABI BigDye Terminator Sequencing kit V2.1; Applied Biosystems) and an automated capillary sequencer (ABI 3730; Applied Biosystems).

RBD assays and MAPK phosphorylation

Ras activation was determined with the minimal RBD of Raf-1 as an activation-specific probe, as described previously (de Rooij and Bos, 1997). Briefly, 293T cells [American Type Culture Collection (ATCC)] were transfected with CMV-promoter-driven expression vectors for N-Ras and mutants. The cells were lysed and active Ras was precipitated with glutathione-agarose beads coupled to GST-RBD. Precipitated N-Ras was detected by western blotting using an N-Ras-specific antibody (Santa Cruz). Zebrafish embryos (24 hpf) were lysed in boiling sample buffer and equal amounts of lysate were loaded onto SDS-PAGE gels. MAPK phosphorylation was established by western blotting using phospho-MAPK-specific mouse monoclonal antibody (mAb; Cell Signaling), and equal loading was monitored using tubulin-specific mouse mAb (Calbiochem), MAPK-specific rabbit mAb (Cell Signaling) and actin-specific rabbit polyclonal antibody (Sigma).

Zebrafish, injections and in situ hybridization

Zebrafish were kept and embryos were raised under standard conditions. Zebrafish were staged as described before (Westerfield, 1995). Constructs encoding human N-Ras and mutants were derived by PCR and verified by sequencing. The wild-type and mutant B-Raf-encoding constructs (Anastasaki et al., 2009) were a gift from Liz Patton. 5′-capped sense RNAs were synthesized using mMessage mMachine kit (Ambion). Synthetic RNA was injected at the one-cell stage. The amount of RNA encoding wild-type N-Ras was titrated down to an amount that did not induce morphological defects by itself (5 pg). Subsequently, 5 pg of all mutants was injected at the one-cell stage. 30 pg RNA encoding wild-type or mutant B-Raf was injected at the one-cell stage (Anastasaki et al., 2009). Phenotypes were assessed at the indicated stages. At 11 hpf, batches of embryos were photo-

graphed and the ratio of major:minor axis of each embryo was determined individually using ImageJ software. Pharmacological inhibitors were added directly to the embryo medium at 4.5 hpf. CI-1040 (Selleck Chemicals) was removed at 5.5 hpf to avoid inadvertent side effects of prolonged treatment, whereas SU5402 (Merck) was left on the embryos for the duration of the experiment. *In situ* hybridizations were performed essentially as described (Thisse et al., 1993) using probes specific for *myod* and *krox20* at the eight-somite stage (~12 hpf) (Li et al., 2008). Quantification of convergence and extension cell-movement defects by analysis of the ratio of the width of *krox20* staining and the length from somite-1 to somite-8 was done using ImageJ software as described before (van Eekelen et al., 2010).

Analysis of cell movement and polarization

Mesendodermal cell tracking was performed exactly as described before (van Eekelen et al., 2010). Briefly, embryos were injected at the one-cell stage with Histone-H1 tagged with Alexa Fluor 488 from Molecular Probes (H1). The embryos were dechorionated and mounted at shield stage in 1% low-melting-point agarose. A Leica SP2 confocal microscope with a 40× objective was used for live imaging and time points were recorded every 2 minutes from shield stage until the one-somite stage. Time-lapse images were analyzed using ImageJ (http://rsbweb.nih.gov/ij/). Following image processing, uniform objects were readily traced, and convergence and extension cell movements quantified. Statistical analysis was performed by the Microsoft Excel Student *t*-test assuming unequal variances with alpha=0.05.

Craniofacial defects

Craniofacial defects were determined by measurement of the ceratohyal angle at 5 dpf. The *Tg(–4.9sox10:EGFP)*^{ba2} transgenic line, in which neural crest cells are marked(Carney et al., 2006), was used, facilitating detection of the ceratohyal. The angle was defined by two lines, one parallel to the left part of the ceratohyal and the other parallel to the right part (cf. Fig. 4C).

Acknowledgments

We thank Elizabeth E. Patton (Edinburgh University, UK) for the B-Raf-V600E construct and Linda A. Winston for critical reading of the manuscript. This work was supported in part by a Marie Curie Research Training Network (PTP-NET/MRTN-CT-2006-035830) and a grant from the Research Council for Earth and Life Sciences (ALW 815.02.007) with financial aid from the Netherlands Organisation for Scientific Research (NWO).

Footnotes

Competing interests
The authors declare that they do not have any competing or financial interests.

Author Contributions
V.R., M.v.E., B.B. and J.d.H. conceived and designed the experiments. V.R., M.v.E., J.O. and B.B. performed the experiments. V.R., M.v.E., H.R., B.B. and J.d.H. analyzed the data. H.G.Y., W.M.N., A.v.H. and I.v.d.B. provided samples. V.R., M.v.E. and J.d.H. wrote the paper.

References

Anastasaki C., Estep A. L., Marais R., Rauen K. A., Patton E. E. (2009). Kinase-activating and kinase-impaired cardio-facio-cutaneous syndrome alleles have activity during zebrafish development and are sensitive to small molecule inhibitors. Hum. Mol. Genet. 18, 2543–2554.

Aoki Y., Niihori T., Narumi Y., Kure S., Matsubara Y. (2008). The RAS/MAPK syndromes: novel roles of the RAS pathway in human genetic disorders. Hum. Mutat. 29, 992–1006.

Bos J. L., Toksoz D., Marshall C. J., Verlaan-de Vries M., Veeneman G. H., van der Eb A. J., van Boom J. H., Janssen J. W., Steenvoorden A. C. (1985). Amino-acid substitutions at codon 13 of the N-ras oncogene in human acute myeloid leukaemia. Nature 315, 726–730.

Bos J. L., Verlaan-de Vries M., van der Eb A. J., Janssen J. W., Delwel R., Lowenberg B., Colly L. P. (1987). Mutations in N-ras predominate in acute myeloid leukemia. Blood 69, 1237–1241.

Carney T. J., Dutton K. A., Greenhill E., Delfino-Machin M., Dufourcq P., Blader

P., Kelsh R. N. (2006). A direct role for Sox10 in specification of neural crest-derived sensory neurons. Development 133, 4619–4630.

Cirstea I. C., Kutsche K., Dvorsky R., Gremer L., Carta C., Horn D., Roberts A. E., Lepri F., Merbitz-Zahradnik T., Konig R., et al. (2010). A restricted spectrum of NRAS mutations causes Noonan syndrome. Nat. Genet. 42, 27–29.

Concha M. L., Adams R. J. (1998). Oriented cell divisions and cellular morphogenesis in the zebrafish gastrula and neurula: a time-lapse analysis. Development 125, 983–994.

Cordeddu V., Di Schiavi E., Pennacchio L. A., Ma'ayan A., Sarkozy A., Fodale V., Cecchetti S., Cardinale A., Martin J., Schackwitz W., et al. (2009). Mutation of SHOC2 promotes aberrant protein N-myristoylation and causes Noonan-like syndrome with loose anagen hair. Nat. Genet. 41, 1022–1026.

de Rooij J., Bos J. L. (1997). Minimal Ras-binding domain of Raf1 can be used as an activation-specific probe for Ras. Oncogene 14, 623–625.

Denayer E., de Ravel T., Legius E. (2008). Clinical and molecular aspects of RAS related disorders. J. Med. Genet. 45, 695–703.

Gelb B. D., Tartaglia M. (2006). Noonan syndrome and related disorders: dysregulated RAS-mitogen activated protein kinase signal transduction. Hum. Mol. Genet. 15 Suppl 2, R220–R226.

Jopling C., den Hertog J. (2005). Fyn/Yes and non-canonical Wnt signalling converge on RhoA in vertebrate gastrulation cell movements. EMBO Rep. 6, 426–431.

Jopling C., van Geemen D., den Hertog J. (2007). Shp2 knockdown and Noonan/LEOPARD mutant Shp2-induced gastrulation defects. PLoS Genet. 3, e225.

Karnoub A. E., Weinberg R. A. (2008). Ras oncogenes: split personalities. Nat. Rev. Mol. Cell Biol. 9, 517–531.

Li C., Inglis P. N., Leitch C. C., Efimenko E., Zaghloul N. A., Mok C. A., Davis E. E., Bialas N. J., Healey M. P., Heon E., et al. (2008). An essential role for DYF-11/MIP-T3 in assembling functional intraflagellar transport complexes. PLoS Genet. 4, e1000044.

Myers D. C., Sepich D. S., Solnica-Krezel L. (2002). Bmp activity gradient regulates convergent extension during zebrafish gastrulation. Dev. Biol. 243, 81–98.

Oliveira J. B., Bidere N., Niemela J. E., Zheng L., Sakai K., Nix C. P., Danner R. L., Barb J., Munson P. J., Puck J. M., et al. (2007). NRAS mutation causes a human autoimmune lymphoproliferative syndrome. Proc. Natl. Acad. Sci. USA 104, 8953–8958.

Pandit B., Sarkozy A., Pennacchio L. A., Carta C., Oishi K., Martinelli S., Pogna E. A., Schackwitz W., Ustaszewska A., Landstrom A., et al. (2007). Gain-of-function RAF1 mutations cause Noonan and LEOPARD syndromes with hypertrophic cardiomyopathy. Nat. Genet. 39, 1007–1012.

Razzaque M. A., Nishizawa T., Komoike Y., Yagi H., Furutani M., Amo R., Kamisago M., Momma K., Katayama H., Nakagawa M., et al. (2007). Germline gain-of-function mutations in RAF1 cause Noonan syndrome. Nat. Genet. 39, 1013–1017.

Roberts A. E., Araki T., Swanson K. D., Montgomery K. T., Schiripo T. A., Joshi V. A., Li L., Yassin Y., Tamburino A. M., Neel B. G., et al. (2007). Germline gain-of-function mutations in SOS1 cause Noonan syndrome. Nat. Genet. 39, 70–74.

Schubbert S., Zenker M., Rowe S. L., Boll S., Klein C., Bollag G., van der Burgt I., Musante L., Kalscheuer V., Wehner L. E., et al. (2006). Germline KRAS mutations cause Noonan syndrome. Nat. Genet. 38, 331–336.

Schubbert S., Shannon K., Bollag G. (2007). Hyperactive Ras in developmental disorders and cancer. Nat. Rev. Cancer 7, 295–308.

Solnica-Krezel L. (2006). Gastrulation in zebrafish – all just about adhesion? Curr. Opin. Genet. Dev. 16, 433–441.

Stewart R. A., Sanda T., Widlund H. R., Zhu S., Swanson K. D., Hurley A. D., Bentires-Alj M., Fisher D. E., Kontaridis M. I., Look A. T., et al. (2010). Phosphatase-dependent and -independent functions of Shp2 in neural crest cells underlie LEOPARD syndrome pathogenesis. Dev. Cell 18, 750–762.

Tartaglia M., Mehler E. L., Goldberg R., Zampino G., Brunner H. G., Kremer H., van der Burgt I., Crosby A. H., Ion A., Jeffery S., et al. (2001). Mutations in PTPN11, encoding the protein tyrosine phosphatase SHP-2, cause Noonan syndrome. Nat. Genet. 29, 465–468.

Tartaglia M., Pennacchio L. A., Zhao C., Yadav K. K., Fodale V., Sarkozy A., Pandit B., Oishi K., Martinelli S., Schackwitz W., et al. (2007). Gain-of-function SOS1 mutations cause a distinctive form of Noonan syndrome. Nat. Genet. 39, 75–79.

Thisse C., Thisse B., Schilling T. F., Postlethwait J. H. (1993). Structure of the zebrafish snail1 gene and its expression in wild-type, spadetail and no tail mutant embryos. Development 119, 1203–1215.

Tidyman W. E., Rauen K. A. (2009). The RASopathies: developmental syndromes of Ras/MAPK pathway dysregulation. Curr. Opin. Genet. Dev. 19, 230–236.

van ‘t Veer L. J., Burgering B. M., Versteeg R., Boot A. J., Ruiter D. J., Osanto S., Schrier P. I., Bos J. L. (1989). N-ras mutations in human cutaneous melanoma from sun-exposed body sites. Mol. Cell Biol. 9, 3114–3116.

van der Burgt I., Kupsky W., Stassou S., Nadroo A., Barroso C., Diem A., Kratz C. P., Dvorsky R., Ahmadian M. R., Zenker M. (2007). Myopathy caused by HRAS germline mutations: implications for disturbed myogenic differentiation in the presence of constitutive HRas activation. J. Med. Genet. 44, 459–462.

van Eekelen M., Runtuwene V., Overvoorde J., den Hertog J. (2010). RPTPalpha and PTPepsilon signaling via Fyn/Yes and RhoA is essential for zebrafish convergence and extension cell movements during gastrulation. Dev. Biol. 340, 626–639.

Westerfield M. (1995). The Zebrafish Book. Eugene, OR: University of Oregon Press.

Zenker M., Lehmann K., Schulz A. L., Barth H., Hansmann D., Koenig R., Korinthenberg R., Kreiss-Nachtsheim M., Meinecke P., Morlot S., et al. (2007). Expansion of the genotypic and phenotypic spectrum in patients with KRAS germline mutations. J. Med. Genet. 44, 131–135.

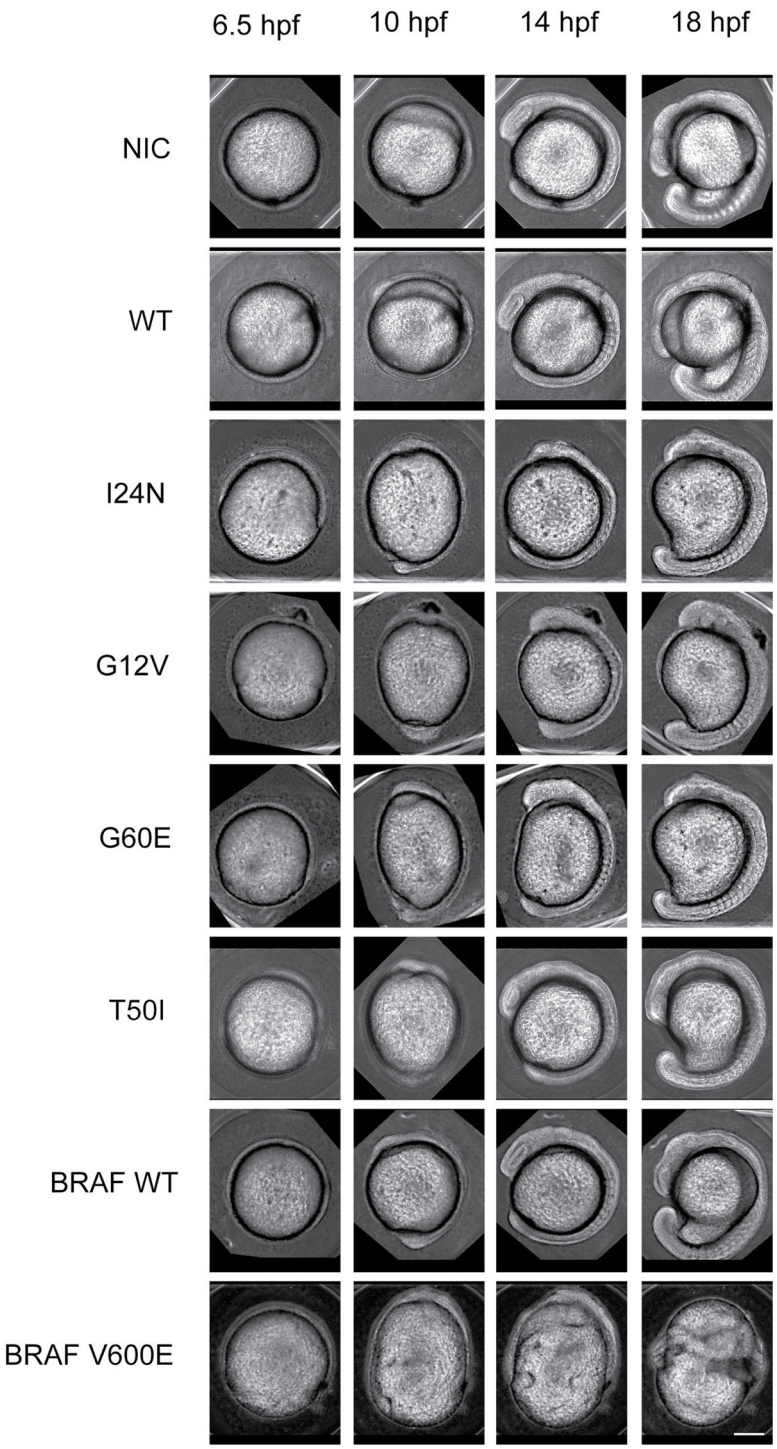

Figure S1. Active N-Ras expression in zebrafish embryos induced developmental defects. Zebrafish embryos were not injected (NIC) or injected at the 1-cell stage with synthetic RNA encoding wild type (WT) or mutant N-Ras-I24N, N-Ras-G12V, N-Ras-G60E, N-Ras-T50I, wild type BRaf (BRAF WT) or mutant BRaf (BRAF V600E). Ten embryos of each group were mounted and their morphology was recorded by time-lapse microscopy from 0 till 18 hpf. Images from representative series are depicted here at 6.5, 10, 14 and 18 hpf. It is noteworthy that at 14 hpf the distance between the anterior-most and posterior-most part of the embryo is enhanced in mutant, active N-Ras injected embryos compared to wild type N-Ras-injected embryos. This is a hallmark of extension defects in gastrulation. The BRaf-V600E injected embryos were severely affected, whereas wild type BRaf injected embryos did not display significant phenotypes. Scale bar is 250 μm.

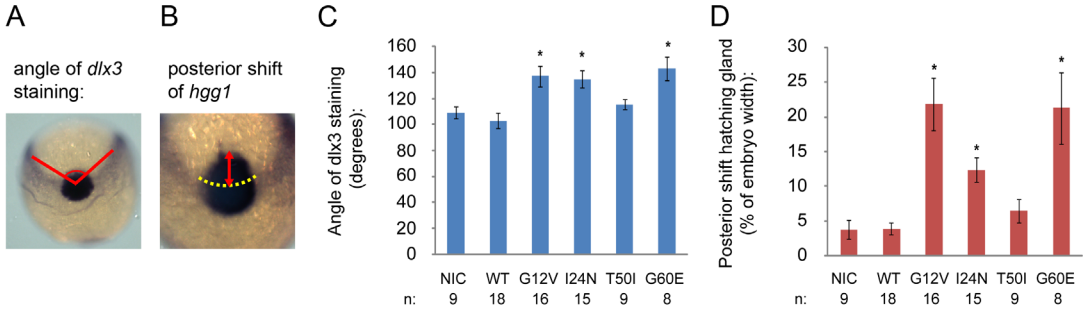

Figure S2. Active N-Ras induced convergence and extension cell movement defects.
(A,B) *In situ* hybridization was done using embryos at the 1-somite stage (~10 hpf) with the *dlx3* and *hgg1* probe. Dorsal views are shown with posterior to the top. Defects in convergence cause widening of the edges of the neural plate (*dlx3*) and hence the angle in (A) is directly proportional to convergence. The position of the precursor of the hatching gland (*hgg1*-staining) relative to the neural plate is directly proportional to extension. The *dlx3*/*hgg1* staining patterns were analyzed using ImageJ software and quantified. (C) The angle of *dlx3* staining and (D) the relative posterior shift of the hatching gland precursor as a proportion of the embryo width of non-injected control (NIC) and embryos injected with synthetic RNA (5 pg) encoding wild type (WT) N-Ras or mutants as indicated were determined. Error bars indicate standard errors of the mean; student's t-tests (2 tailed, assuming unequal variance) were performed between mutant and wild type N-Ras-injected groups, * indicates a P value<0.001. The total number of embryos that were used for the analyses are indicated.

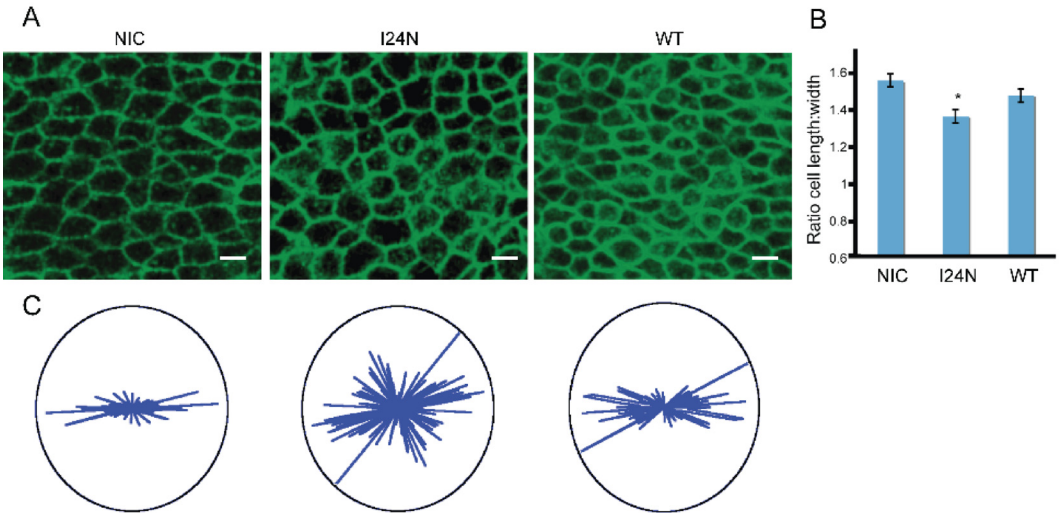

Figure S3. Impaired cell polarization in response to N-RAS-I24N.
Zebrafish embryos were injected with YFP-CAAX and N-RAS-I24N or wild type N-RAS (WT). Embryos were mounted and imaged at late gastrulation stage posterior of the future site of the first somite in the region next to the notochord. (A) Depicted are representative images of non-injected control (NIC), N-RAS-I24N-injected and wild type N-RAS-injected embryos. Scale bar is 10 µm. (B) Length and width of the cells were determined and the ratios are plotted. Error bars represent standard deviation. A student's t-test was performed; asterisk indicates significant difference, P<0.001. (C) The angles of cells towards the notochord were determined using ImageJ software and are plotted in a rose diagram.